Optimized Fenton-like reaction pathways by Ov-contained ZnO@nitrogen-rich porous carbon: Electron transfer and $^1O_2$ triggered non-radical process

Zhenfeng Zhang[a] [1], Tianli Xiong[a] [1], Haihao Peng[b] [1], Honglin Zhang[a], Siying He[a], Xuran Liu[c],

Yanan Liu[a], Wenyi Feng[a], Zhaohui Yang[a], Weiping Xiong[a]*

[a] College of Environmental Science and Engineering and Key Laboratory of Environmental

Biology and Pollution Control (Ministry of Education), Hunan University, Changsha 410082,

PR China

[b] School of Chemistry and Chemical Engineering / Institute of Clean Energy and Materials /

Guangzhou Key Laboratory for Clean Energy and Materials, Guangzhou University,

Guangzhou 510006, P. R. China

[c] Department of Civil and Environmental Engineering, The Hong Kong Polytechnic

University, Hung Hom, Kowloon, Hong Kong, SAR, PR China

CONTENTS

Catalysts and methods

Supplementary Note 1: Catalysts and chemicals.

Zinc oxide (ZnO), 2-methylimidazole (HmIm), Zinc nitrate hexahydrate (Zn(NO$_3$)$_2$•6H$_2$O), N, N-Dimethylformamide (DMF), Methanol (MeOH), Ethanol absolute, Sodium persulfate (PDS), Sulfamethazine (SMZ). Sodium hydroxide (NaOH) and hydrochloric acid (HCl) were used to adjust pH. Sulfamethizole (SMT), Tetracycline Hydrochloride (TC), Norfloxacin (NOF), Phenol, 4-Chlorophenol (4-CP), Benzoic acid (BA), and Carbamazepine (CBZ), Sodium sulfate anhydrous (Na$_2$SO$_4$), Naphthol (C$_{10}$H$_8$O). Sodium chloride (NaCl), Sodium dihydrogen phosphate (NaH$_2$PO$_4$), Sodium bicarbonate (NaHCO$_3$), and Humic acid (HA) were used to represent natural background ions. Tert-butanol (BPA), Sodium azide (NaN$_3$), 1,4-Benzoquinone (BQ), potassium dichromate (K$_2$CrO$_4$), Phenyl methyl sulfoxide (PMSO), Nitrotetrazolium Blue chloride (NBT) and 1,3-Diphenylisobenzofuran (DPBF) were used as quenching or trapping agent. Methanol (MeOH) and acetonitrile (ACN) of high-performance liquid chromatography (HPLC) grade were purchased from TEDIA (USA). All the solutions were prepared with ultrapure water (18.25 MΩ) purified by a Mili-Q system. All chemicals were of analytical grade and were directly used without further purification.

Supplementary Note 2: Preparation of catalysts.

Preparation of ZnO @ NPC: Zinc oxide nanosheets (1 mmol) and 2-methimidazole (4 mmol) were added to the 64 ml DMF / H_2O mixture (volume ratio of DMF to water is 3:1), stirred and sonicated for 10 min, and the mixture was transferred to 100 ml Teflon-lining steel autoclave and heated to 70°C for 24 hours. [1, 2] After natural cooling, the white sample was washed three times with DMF and Ethanol, and dried in Vacuum ovens overnight at 60°C, then the resulting production was ZnO@ZIF-8. The ZnO@ZIF-8 after drying was ground and calcined at 900°C (with the ramping rate of 5°C min^{-1}) in an Ar atmosphere for 120 min in the tubular furnace. Then the final ZnO@NPC was obtained. [3]

Preparation of NPC: 2-methimidazole (16 mmol) and $ZnNO_3 \cdot 6H_2O$ (4 mmol) were dissolved in 50 ml MeOH, stirred and sonicated for 10 min, then transferred to 100 ml Teflon-lined steel autoclave and heated to 120°C for 4 hours. After natural cooling, the white sample was washed three times with MeOH and Ethanol and dried in Vacuum ovens overnight at 60°C, then the resulting production was ZIF-8. The ZIF-8 after drying was ground and calcined at 900°C (with the ramping rate of 5°C/min) in Ar atmosphere for 120 min in the tubular furnace. Then the final NPC was obtained. [2]

Supplementary Note 3: Characterization.

X-ray diffraction (XRD) patterns were recorded on an X-ray diffractometer with Cu-Kα radiation, λ = 1.5406 Å (XRD, Rigaku Ultima IV, Japan). X-ray photoelectron spectroscopy

(XPS) experiments were carried out using a Thermo Scientific K-Alpha with an Al anode at 15kV 50W radiation source, and all the peak were calibrated by the C 1s spectrum at 284.8 eV. Zeta potential was measured by Zetapotential analyzer （Zetasizer Nano ZS， US）. Catalysts morphology was taken by Scanning electron microscopy (SEM, ZEISS Sigma 300), with an acceleration voltage of 3 KV, and Transmission Electron Microscope (TEM, JEM-F200 Japan). Thermogravimetry Analysis (TG, STAZ500A-O277-N) was measured in an air atmosphere with a rate of 5°C/min and a temperature range of 50-800°C. The pore sizes and pore volumes of samples were carried out using the Brunauer-Emmett-Teller (BET) instrument (ASAP 2020 plus) based on N_2 adsorption-desorption isotherms tested at 77.3 K. Fourier transform infrared spectrometer (Thermo Scientific Nicolet iS20) was used for Fourier Transform Infrared Spectra (FT-IR) spectra that were performed in a KBr sheet in a region of 400~4000 cm^{-1} to qualitatively measure the surface functional groups of catalyst. Raman spectra were acquired from a Microscopic confocal Raman spectrometer (Thermo Scientific DXR 3Xi, USA) equipped with a 532 nm laser at an ambient temperature. Electron paramagnetic resonance (EPR) spectra were performed on a Bruker A300 spectrometer (Bruker EMXplus-6/1, Germany) at room temperature. The total organic carbon (TOC) was measured by an analyzer (TOC-VCPH, Japan).

Supplementary Note 4: Analytical methods of organic compounds.

Target contaminant (SMZ) was determined on an HPLC system (1200, Agilent Technology, USA) equipped with a C18 column (4.6 × 250 mm, 5 um). The mobile phase was acetonitrile/water (35:65, v/v%) with a flow rate of 1.0 ml/min, the temperature was 30°C, and the

detection wavelength was selected at 266 nm. Sulfamethizole (SMT), Tetracycline Hydrochloride (TC), Norfloxacin (NOF), Phenol, 4-Chlorophenol (4-CP), Benzoic acid (BA), Carbamazepine (CBZ) and PMSO/PMSO$_2$ were analyzed by the HPLC system, and detection method details are provided in Table S6.

The degradation intermediates of SMZ were identified by UPLC system (Agilent 1290/6460, USA) connected with a triple quadrupole mass spectrometer (Triple Quad MS, USA). The HPLC column was an Agilent Kromasil C18 column (4.6 x 100 mm), column temperature was 40°C. The flow rate was set to 0.45 ml/min and the injection volume was 10 µL. The mobile phases consisted of acetonitrile (A) and water (B). The gradient elution was initially 20% A, 80%B; held for 1 min, and rose to 100% A within 6 min, then mobile phase B returned to 20% in 10 min, held for 2 min for equilibration of the column. The MS system was operated in ESI mode using electrospray interface. The ionization source conditions used were as follows: EIS was performed at 3.8 kV and 350°C, sheath gas 11 L/min at a temperature of 350°C, and the nebulizer pressure 35 psi. The mass range between m/z 50 and m/z 600 was scanned to obtain full scan mass spectra.

Supplementary Note 5: Catalytic activity experiments.

The catalytic performance was evaluated in a 50 ml conical flask at a thermostatic shaker with a shaking rate of 150 rpm. Typically, catalysts (5 mg) were added into the aqueous solution of SMZ (50 ml, 20 mg L^{-1}), then the suspension was shaken for 15 min to establish an adsorption-desorption equilibrium. Following the PDS (0.8 mM) was added into the suspension to trigger the degradation reaction. Subsequently, at specific time intervals (5, 10, 15, 30, 45, 75 min), 0.8 mL

water samples were taken out from the conical flask and filtered through a 0.22 um polytetrafluoroethylene (PTFE) filter, then mixed with 0.8 mL methanol (methanol act as quenching and diluting agent) for HPLC system. To explore the effect of initial pH on catalytic performance, the pH value of SMZ aqueous solution was set from 2-12 spaced by 2, in which the desired value was adjusted by NaOH and HCl solution. To indicate the resistance of the ZnO@NPC/PDS system, Cl^- (5 mM), $H_2PO_4^-$ (5 mM), HCO_3^- (5 mM), and HA (10 mg L^{-1}) were added to the SMZ solution to carry out the experiments. The methods of degradation tests for the other pollutants including Sulfamethizole (SMT), Tetracycline Hydrochloride (TC), Norfloxacin (NOF), Phenol, 4-Chlorophenol (4-CP), Benzoic acid (BA), and Carbamazepine (CBZ) were the same as those of SMZ, and the concentrations were all 20 mg/L. Quenching experiments have been carried out to identify ROS, methanol, TBA, NaN_3, p-BQ, and K_2CrO_4 were served as the scavengers for $\cdot OH$, $SO_4^{\cdot-}$, $^1O_2$, $O_2^{\cdot-}$, and e^-, respectively. The DPBF and NBT were used as capture agents to confirm the production of $^1O_2$ and $O_2^{\cdot-}$, respectively.

Then, the kinetic rate constants (K_{obs}) of pollutant degradation were further analyzed. The kinetics equation is as follows:

$$\ln \left(C_t / C_0 \right) = - K_{obs} \times t$$

Where C_0 is the initial organic pollutant concentration, C_t is the concentration at a reaction time during the degradation process, t is reaction time.

Typically, adsorption experiments were performed as follows: catalysts (5 mg) were added into the aqueous solution of SMZ (50 ml, 20 mg/L), Subsequently, at specific time intervals (15, 30, 45, 60, 75 min), 0.8 mL water samples were taken out from the conical flask and filtered through

a 0.22 µm PTFE filter, then mixed with 0.8 mL methanol (methanol act as quenching and diluting

agent) for HPLC system.

Then, the adsorption kinetic (K) of pollutants was analyzed.

The First-order kinetic:

$$q_t = q_e - q_e e^{-K_1 t}$$

The second-order kinetic:

$$\frac{t}{q_t} = \frac{1}{K_2 q_e^2} + \frac{t}{q_e}$$

q_t is adsorption capacity, q_e is the adsorption capacity at equilibrium, K_n is the kinetic rate

constants of pollutants adsorption, t is reaction time.

Supplementary Note 6: Electrochemical test.

For identification of the direct electron-transfer process during PDS activation, electrochemical

measurements including electrochemical impedance spectroscopy (EIS), linear sweep

voltammetry (LSV), and i-t curves were measured by an electrochemical workstation (CHI760E

China). Firstly, 1 mg ZnO@NPC or NPC was dispersed into 100 mL naphthol-ethyl alcohol

solution (5: 95, v/v%) with 30 min ultrasonic and shake treatment. Then, the mixture was dropped

onto the conductive glass (1×2 cm) and dried for 20 min, repeated the above steps three times to

make three electrode sheets. Electrochemical measurements were conducted in three-electrode cell

with Pt electrode as counter electrode and Ag/AgCl electrode as the reference electrode. EIS was

carried out at Na_2SO_4 solution (0.2 M), the initial potential was 0.22 V, and the frequency range

was from 100 to 1000000 Hz. LSV was performed with a reaction potential of 0-1 V and a scan

rate of 0.05 V/S in different reaction solutions (0.2 M Na_2SO_4, 0.8 mM PDS, 20 mg/L SMZ, 20 mg/L SMZ+ 0.8 mM PDS). I-t curves were also measured in Na_2SO_4 solution (0.2 M) with an initial potential of 0.3 V, PDS and SMZ were added around 130 s and 280 s, respectively.

Galvanic oxidation process (GOP) was carried out in two half cells which added 50 mL PDS solution (0.8 mM) and SMZ solution (20 mg/L), respectively, and connected the reaction system via a KCl agar salt bridge. An ammeter was used to monitor the relative current during the reaction. 5 mg of ZnO@NPC was dispersed into 400 µL of naphthol-ethyl alcohol solution (5: 95, v/v%) and then uniformly applying it on the graphite electrode sheet and drying it for 20 min. The specific installation is shown in Figure S25.

## Supplementary Note 7: Toxicity evaluation method.

In order to have a comprehensive understanding of degradation intermediates, we performed a toxicity assessment. Firstly, the toxicity of SMZ and the oxidation by-products were evaluated by Toxicity Estimation Software Tool (T.E.S.T) program developed by the QSAR model. Since the partial substance in our experiment, without experimental value and predicted value in related data, the method of nearest neighbor was used for individual predictions (with the highest Similarity coefficient). Acute toxicity of Fathead minnow LC_{50} (96 h), Daphnia magna LC_{50} (48 h), and T. Pyriformis LC_{50} (48 h), Bioconcentration factor, developmental toxicity value, and mutagenicity value, of degradation intermediates were assessed via T.E.S.T.

Secondly, the phytotoxicity of SMZ and degradation productions to lucerne (*Medicago sativa L*) seeds was tested by seed germination and radicle elongation tests. Three sets of samples were

set up including pure water, SMZ solution (20 mg/L), and end-products. Pure water was used as the control, end-products were decomposed by the ZnO@NPC/PDS/SMZ system. The seeds were cleaned with pure water several times. Two filter papers were placed in a petri dish, and 20 seeds were placed in each petri dish with 5 mL solution (60 seeds in each group). All the experimental groups and control group were placed in a dark incubator at 25 °C for 120 h (replenish solution every 24 h). The germination rate and radicle length of germinated seeds in all groups were counted and calculated. The periosteum length of lucerne was analyzed by Statistical significance by IBM SPSS Statistics 26 software. Specific results were shown in Figure S26 and Table S5.

Supplementary Note 8: Measurement methods of PDS

The method for measuring the concentration of PDS in solution was consulted from wang et al. [4] and Yang et al. [5] The $S_2O_5^{2-}$ can react with KI while the $NaHCO_3$ is present, forming a pale yellow color that can be identified on a UV spectrophotometer at 352 nm. The color rendering agent was compounded with KI (92.22 g/L) and $NaHCO_3$ (4.44 g/L). The reaction equation is as follows:

$$S_2O_8^{2-} + 2I^- \rightarrow 2SO_4^{2-} + I_2$$
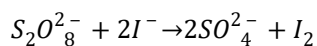
In our experiment, at specific time intervals (5, 10, 15, 30, 45, 75 min), 0.5 mL water samples were taken from the flask and filtered through a 0.22 um PTFE filter, then mixed with 4.5 mL color rendering agent. It was mixed thoroughly and left to stand for 20 min, and then detected at a wavelength of 352 nm.

Supplementary Note 9: Nitro-blue tetrazolium (NBT) colorimetric method for determination of $O_2^{\bullet-}$ formation.

Nitrotetrazolium blue chloride (NBT) was a probe to detect $O_2^{\bullet-}$. 15 mg catalyst, 50 ml NBT solution (0.25 mM), and 0.8 mM PDS were added into a conical flask. At specific time intervals (5, 10, 15, 30, 45, 75 min), 3 mL water samples were taken out from the flask and filtered through a 0.22 μm PDFE filter. The NBT was reduced by $O_2^{\bullet-}$ to formazan, which was measured by UV spectrophotometer at $\lambda = 530$ nm. The result is shown in the Figure 4a and S17.

Supplementary Note 10: 1,3-Diphenylisobenzofuran (DPBF) colorimetric method for determination of $^1O_2$ formation.

DPBF was used as a probe of $^1O_2$, in this work, 5 mg catalyst, 50 mL DPBF (0.5 mM), and 0.8 mM PDS were added into a conical flask. At specific time intervals (5, 10, 15, 30, 45, 75 min), 3 mL samples were taken out from the flask and filtered through a 0.22 μm PDFE filter, The DPBF was measured by UV spectrophotometer at $\lambda = 411$ nm. The result is shown in Figure S13.

Supplementary Note 11: EPR analysis for ROS.

EPR was employed to detect Reactive Oxygen Species (ROS) at environmental temperatures in our systems. Specifically, for the identification in ZnO@NPC/PDS system, 2 mg ZnO@NPC and 3 mg PDS were added into 10 ml water (for $\bullet OH/SO_4^{\bullet-}$, $^1O_2$) or 10 mL methanol (for $O_2^{\bullet-}$). 2,2,6,6-tetramethyl- 4-piperidinol (TEMP) (100 mM) were used as $^1O_2$ spin-trapping agents with the

formation of 2,2,6,6-tetramethyl-4-piperidinol-N-oxyl (TEMPO) adduct. 5,5-dimethyl-1-pyrroline-N-oxide (DMPO) (100 mM) were used as spin-trapping agents to identify •OH/SO$_4^{•-}$ in ZnO@NPC/PDS/water system and O$_2^{•-}$ in ZnO@NPC/PDS/methanol system. The ^{1}O$_2$ in the ZnO@NPC/PDS/SMZ system was detected by the same method after replacing pure water with SMZ solution. Control groups were measured in pure water and methanol solution with PDS only.

Supplementary Note 12: Phenyl methyl sulfoxide (PMSO) oxidation experiment.

PMSO was employed as a probe of high-valent metal, the sulfoxides could be oxidized by high-valent metal to form intermediate methyl phenyl sulfone (PMSO$_2$). In the experiment, 5 mg ZnO@NPC, 50 mL PMSO (0.1 mM), and 0.8 mM PDS were added into a conical flask. At specific time intervals (5, 10, 15, 30, 45, 75 min), 0.8 mL samples were taken out from the flask and filtered through a 0.22 µm PTFE filter. The PMSO and PMSO$_2$ were measured by the HPLC system (Table S6). And the result is shown in the Supplementary Figure S16.

Supplementary Note 13: Vienna Ab initio Simulation Package.

Density functional theory (DFT) calculations were obtained with the help of the Science Compass. DFT was carried out in the Vienna ab initio simulation package (VASP) based on the plane-wave basis sets with the projector augmented-wave method. First, the model construction under these conditions, a vacuum region of about 18 Å was applied to avoid the interaction between adjacent images. The unsaturated Zn sites on the bottom of ZnO (101) surface were

coordinated with pseudo hydrogen with 0.5 charge. The ZnN$_4$-ZnO (101-Ov) heterojunction was built based on the lattice parameter of ZnO. To treat the mismatch of ZnO (101) surface. The ZnN$_4$ loaded graphene was truncated and end-capped with hydrogen atoms. The energy cutoff was set to be 450 eV. The Brillouin-zone integration was sampled with a Γ point ($1 \times 1 \times 1$). The structures were fully relaxed until the maximum force on each atom was less than 0.02 eV/Å, and the energy convergent standard was 10^{-6} eV. Then the adsorption energy E$_{ads}$ can be defined as

$$E_{ads} = E_{*+PDS} - E_* - E_{PDS}$$

Where E_{*+PDS} stands for the energy of the heterojunction with the adsorbed PDS molecule, E_* is the energy of a clean heterojunction, and E_{PDS} is the energy of a PDS molecule under vacuum.

The charge density difference (CDD) can be defined as
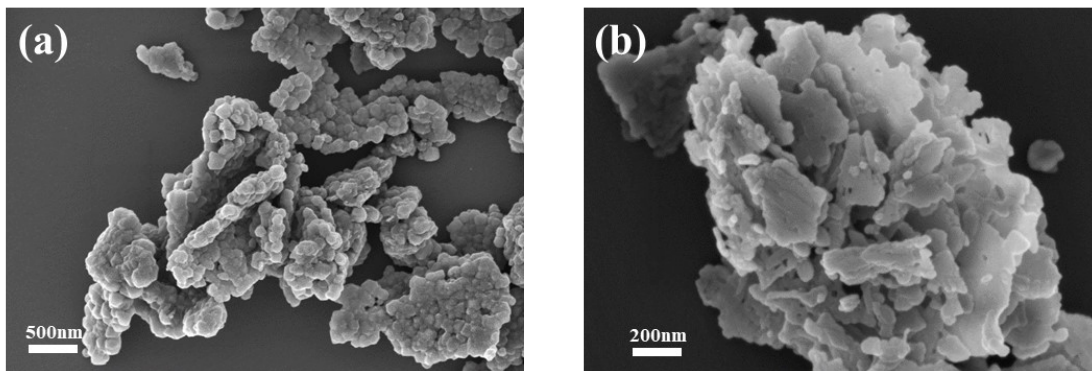
$$\Delta\rho = \rho_{AB} - \rho_A - \rho_B$$

Where ρ_{AB}, ρ_A, and ρ_B are the electron densities of the assigned structures and its counterparts.

Figure S1: The synthesis procedure of NPC
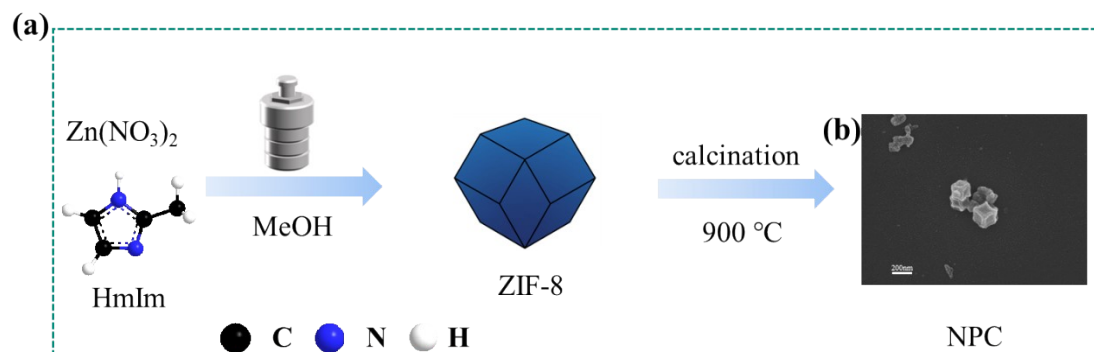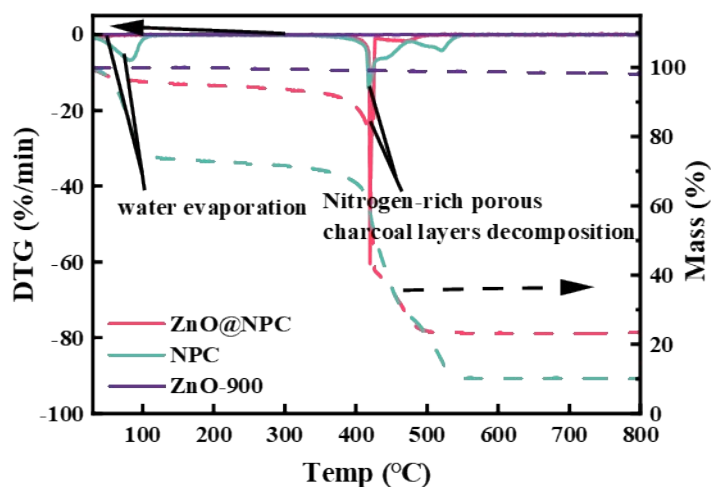

(a) The synthesis procedure of NPC, (b) SEM of NPC

Figure S2: SEM

(a) ZnO@ZIF-8, (b) ZnO nanosheet

# Figure S3: Thermogravimetry Analysis

NOTE: The decomposition steps were observed by pyrolyzing the catalysts in an air atmosphere, as shown in the figure, the first decomposition of NPC and ZnO@NPC occurred at 80 °C and was attributed to the deposition of water. The second decomposition of NPC occurred at 400 °C and was mainly attributed to the decomposition of the carbon layer, which retained only 10 % of the original mass after decomposition. Meanwhile, ZnO@NPC also decomposed at 400 °C and retained 22% of its original mass, while ZnO hardly decomposed at all. These indicated that ZnO@NPC consists of a nitrogen-rich porous carbon layer and ZnO, which was consistent with the results of TEM.

14

Figure S4: Pore size distribution
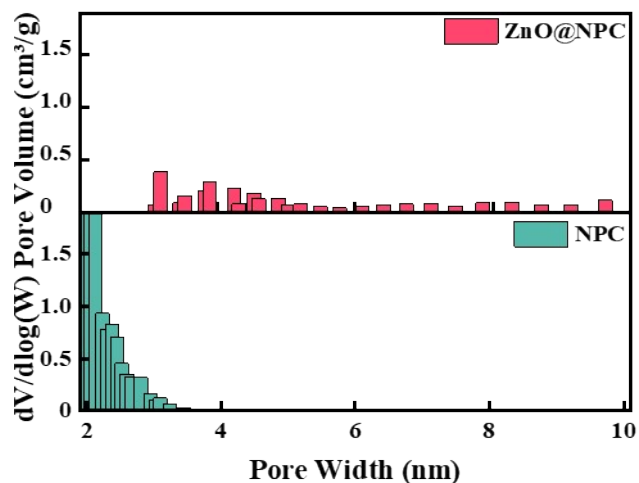
NOTE: The pore sizes of NPC were concentrated in 2-4 nm, and the single pore size was harmful to the diffusion of pollutants and PDS. The pore sizes of ZnO@NPC were uniformly distributed in all particle sizes, and the pollutants and oxidants could be diffused step-by-step, which accelerated the reaction rate and improved catalytic performance. The pore size distribution results were consistent with the adsorption isotherm property of catalysts.

Figure S5: XRD of ZnO@NPC
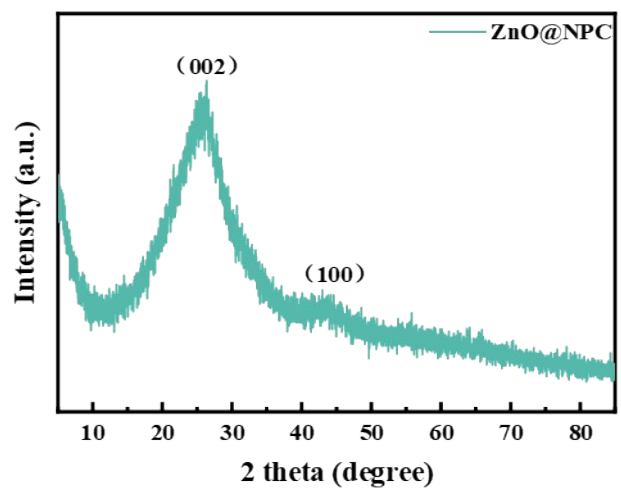
Figure S6: XPS
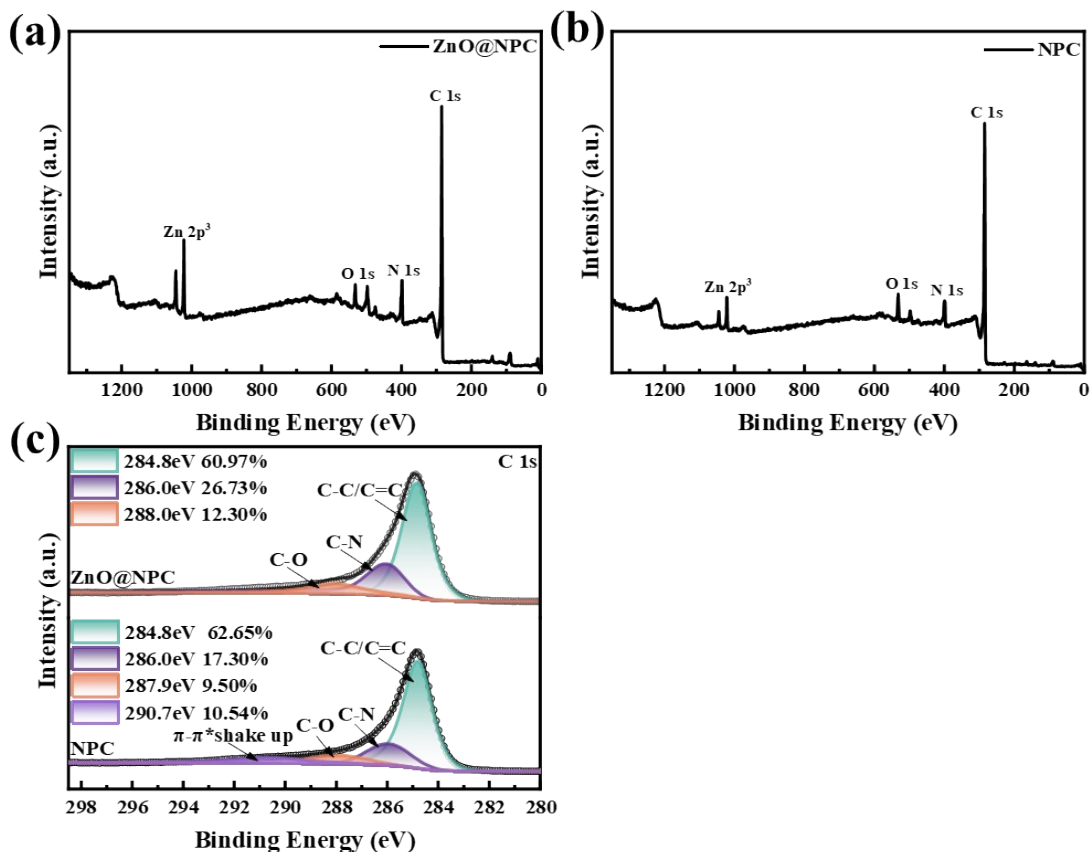
XPS: (a) ZnO@NPC, (b) NPC, (c) C 1s of ZnO@NPC and NPC

NOTE: The main elements of ZnO@NPC and NPC were C, N, O, and Zn. The high-resolution C 1s spectrum of ZnO@NPC displayed three main peaks at 284.8, 286.0, and 288.0 eV which ascribed to the form of C=C/C-C, C-N, and C-O, respectively. However, π-π^* shake up was identified in the high-resolution C 1s spectrum of NPC, which made the composition of NPC more stable with fewer active sites, and lower catalytic performance. However, the presence of π-π bonds was more favorable to the adsorption property of the catalyst. [5, 6]

Figure S7: Screening of reaction conditions
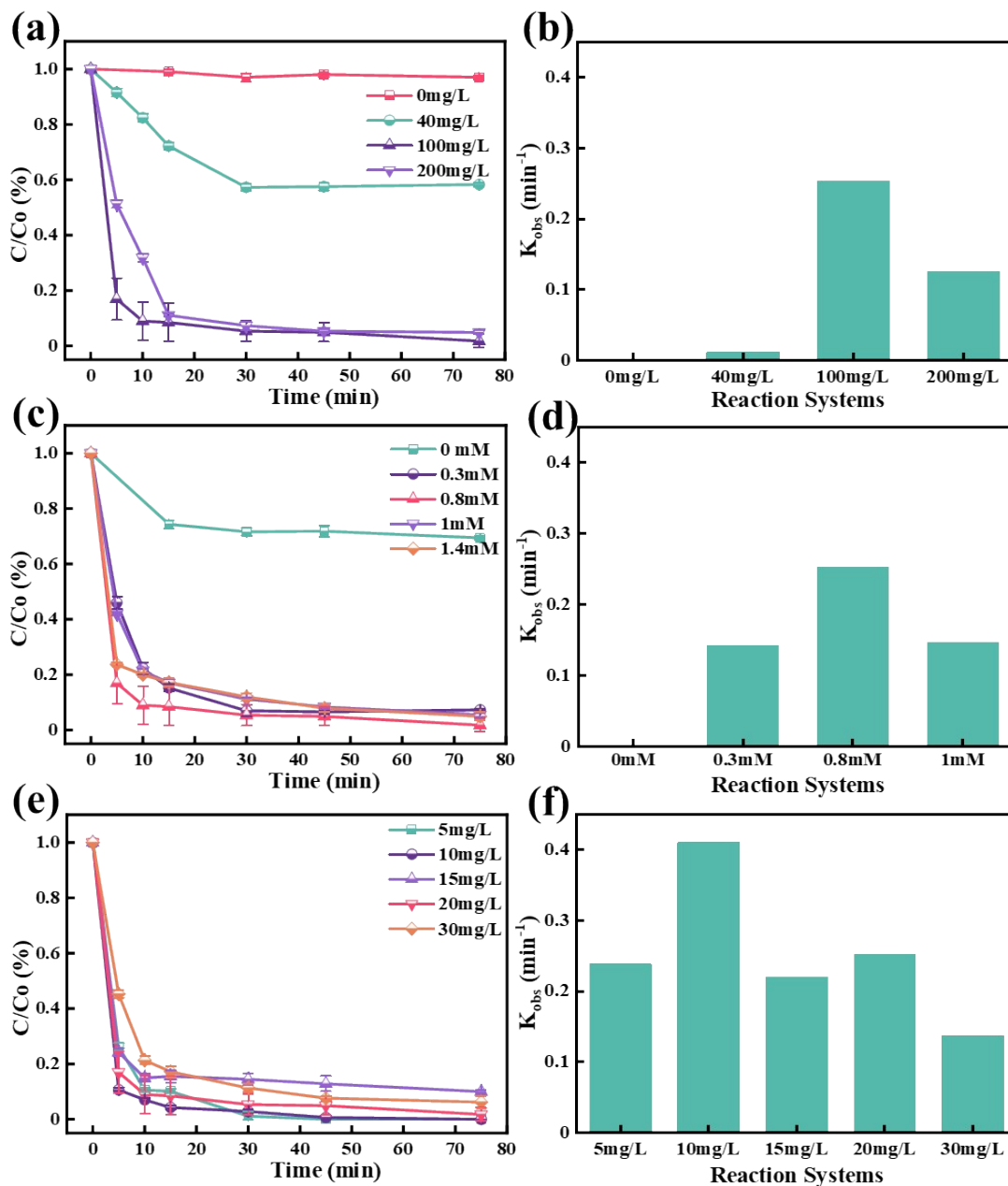
Graph of (a) degradation effect and (b) degradation rate for different catalyst qualities, Graph of

(c) degradation effect and (d) degradation rate for different PDS concentrations, Graph of (e)

degradation effect and (f) degradation rate for different SMZ concentrations. Degradation

conditions: ZnO@NPC = 0.1 mg/L (in c, d, e, f), PDS = 0.8 mM (in a, b, e, f), SMZ = 20 mg/L

(in a, b, c, d).

NOTE: The catalytic performance was evaluated in a 50 ml conical flask at a thermostatic shaker with a shaking rate of 150 rpm. By comparing the degradation effect and rate of different ZnO@NPC quality, it was found that the fastest degradation rate was achieved at 100 mg/L and further increasing the quality of ZnO@NPC was not significant. The removal efficiency of SMZ was only 3.5% without ZnO@NPC, indicating that the activation effect of pure PDS was negligible and ZnO@NPC played a key role in the reaction system. SMZ could be degraded rapidly within 15 min with PDS and ZnO@NPC, and the fastest degradation rate was reached when PDS was 0.8mM. Whereas SMZ was removed only 30% by adsorption. As shown in Figure S7e, and S7f, it could be found that SMZ was removed rapidly by the ZnO@NPC/PDS system. **The optimal reaction conditions were as follows: Catalyst = 100 mg/L, PDS = 0.8 mM, SMZ = 20 mg/L.**

Figure S8: The fitting of adsorption curves and degradation rate (K_{obs}) of different reaction systems
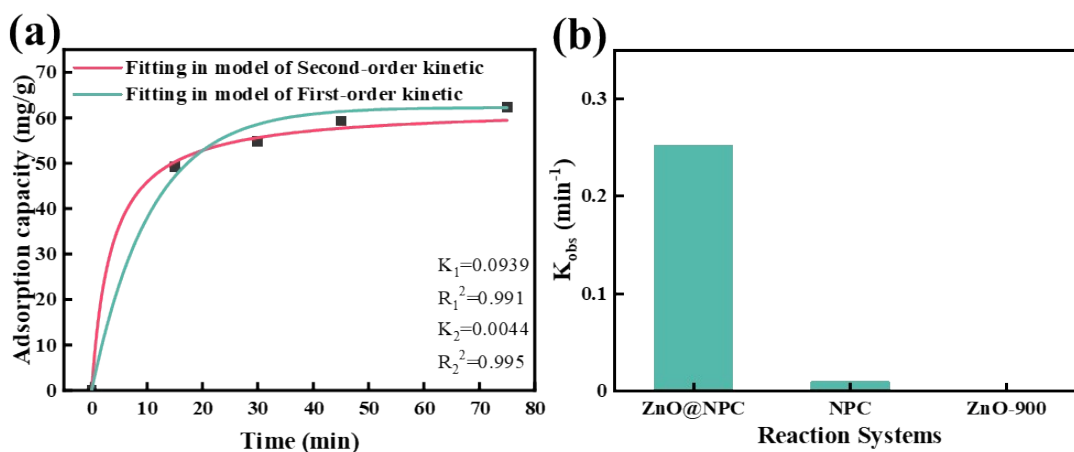
(a) The fitting of adsorption curves, (b) K_{obs} of different reaction systems

NOTE: The adsorption was fitted so that if the kinetics obeyed First-order, the adsorption was usually physisorption, if it obeyed second-order, it was chemisorption. By comparing the results of fitting in different models (Figure S8a), it was found that the adsorption was chemisorption and the adsorption constant (K_2) was 0.0044 because the R^2 value of the second-order kinetic was greater than the first-order kinetic. From the K_{obs} of the different reaction systems, it was clearly observed that the ZnO@NPC/PDS system had the highest degradation rate, which was 12 times higher than that of the NPC/PDS system. The ZnO/PDS system was almost incapable of removing the pollutants, with a degradation rate of zero.

Figure S9: K_{obs} in different works
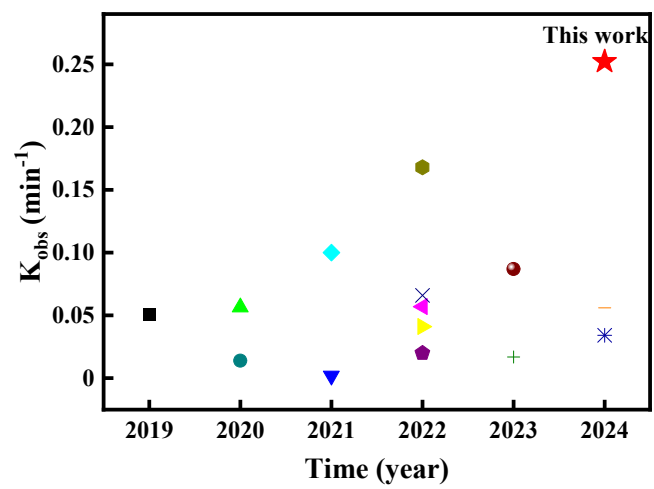
Figure S10: The effect of initial pH
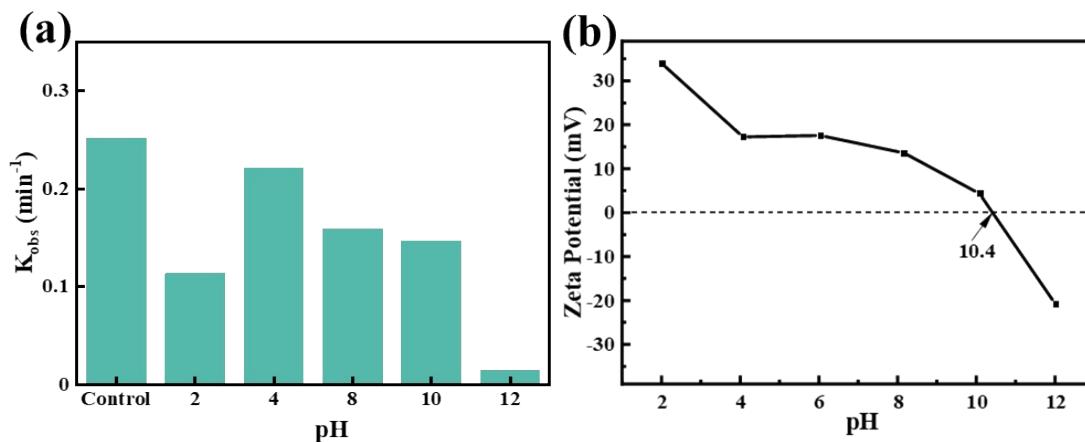
(a) K_{obs} of different initial pH values, (b) zetasizer potential

NOTE: It could be observed from Figure S10a that the degradation performance of the ZnO@NPC of initial pH was almost invariable in the range of 2-10. At the extremely alkaline conditions of pH = 12, the decrease in the degradation rate of the ZnO@NPC/PDS system might be attributed to the change of surface structure and electron distribution, which can be evident from the ZATE potential (Figure S10b). It could be seen that ZnO@NPC was relatively stable under acidic conditions. When pH > 10.4, the surface properties and structure of ZnO@NPC changed, which made the catalytic performance weaker.

# Figure S11: K_{obs} of different reaction systems
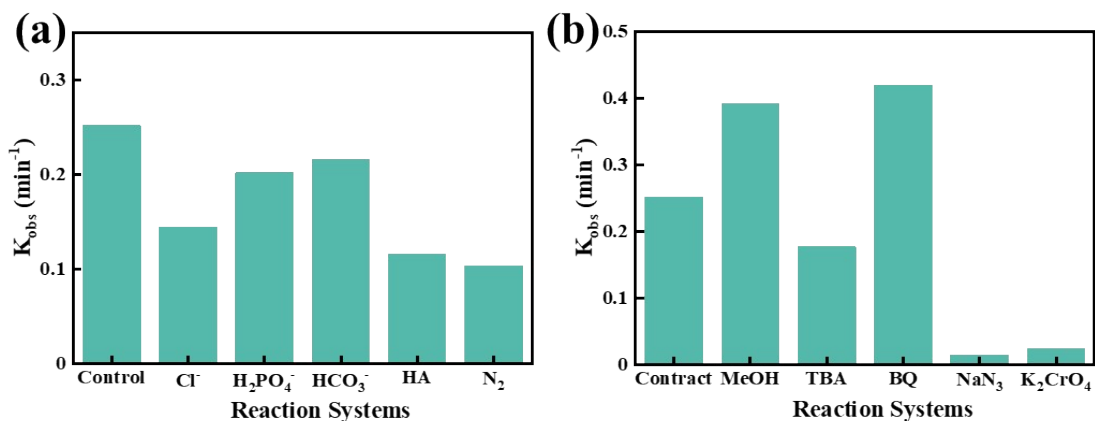
(a) K_{obs} of various co-existed ions. (b) K_{obs} of different quenching agents. Degradation conditions: ZnO@NPC = 0.1 g/L, PDS = 0.8 mM, SMZ = 20 mg/L, quenching agents: MeOH = 1 M, TBA = 1 M, BQ = 10 mM, NaN_3 = 50 mM, K_2CrO_4 = 5 mM, temp = 25°C, shake 150 rpm.

NOTE: The degradation performance of ZnO@NPC was unaffected with the presence of interfering ions. This indirectly proved that the ZnO@NPC/PDS system was not dominated by free radicals which were easily consumed by co-existing ions and HA.

Figure S12: Influence of different quenching agents in NPC/PDS/SMZ system
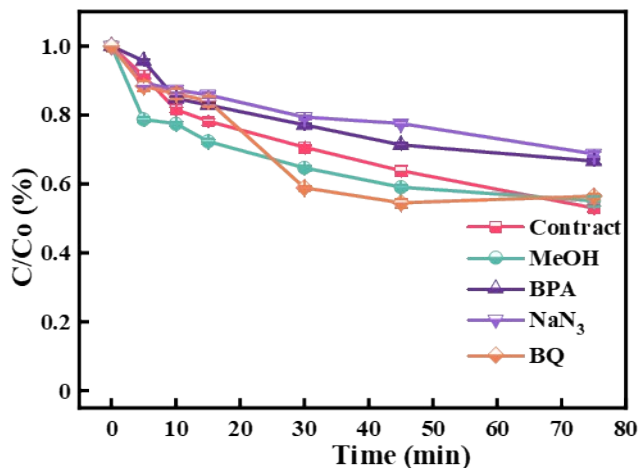
Degradation conditions: NPC = 0.1 g/L, PDS = 0.8 mM, SMZ = 20 mg/L, MeOH = 1 M, BPA =

1 M, NaN$_3$/BQ = 10 mM, temp = 25°C, shake 150 rpm

NOTE: It could be observed that the degradation effect of the NPC/PDS system was inhibited by BPA and NaN$_3$, indicating the presence of •OH and $^1O_2$ in the system. The low degradation effect of SMZ in the NPC/PDS system suggested that the production rate and amount of •OH and $^1O_2$ were limited.

Figure S13: The degradation of DPBF in different systems
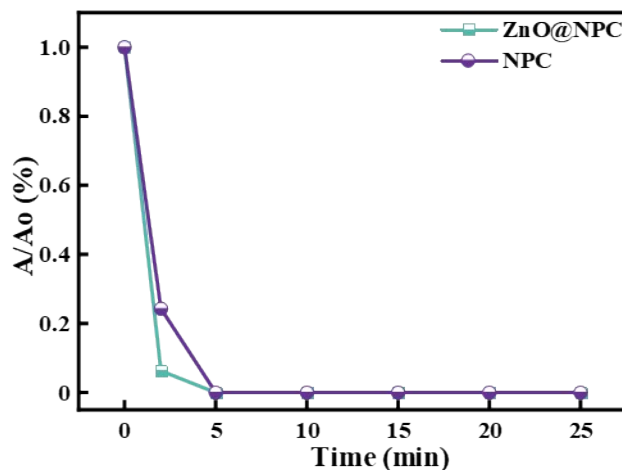
Degradation conditions: Catalysts (ZnO@NPC, NPC) = 0.1 g/L, PDS = 0.8 mM, DPBF = 0.5

mM, temp = 25°C, shake 150 rpm

NOTE: The removal of DPBF within 3 minutes indicated that $^1O_2$ was present and could be produced rapidly in the ZnO@NPC/PDS system. While $^1O_2$ was produced at a low rate in the NPC/PDS system, which was consistent with the quenching results.

# Figure S14: The EPR detection results of the ZnO@NPC/PDS system
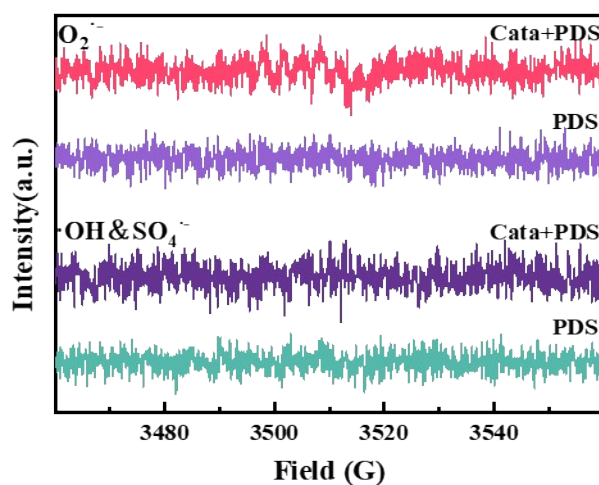
NOTE: The absence of signals of $O_2^{\bullet-}$ •OH and $SO_4^{\bullet-}$ further indicated that there was no free radicals in the ZnO@NPC/PDS system.

Figure S15: PMSO trap experiments in different systems
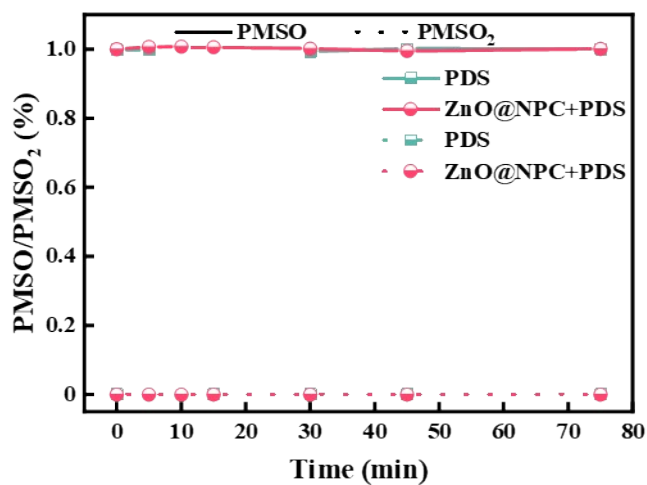
NOTE: As shown in the picture, the solid lines represented the change of PMSO and the dotted lines represented the change of $PMSO_2$ (the oxidation product of PMSO), the reaction process did not produce $PMSO_2$ indicating that no high-valent metal was present in the ZnO@NPC/PDS system.

Figure S16: The degradation of NBT in the NPC/PDS system
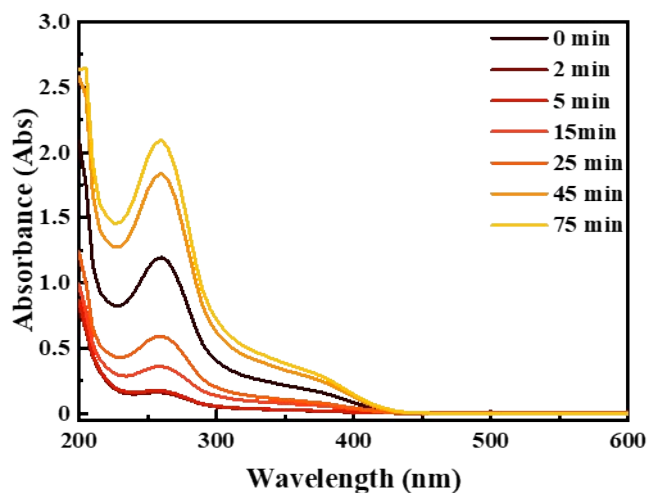
Degradation conditions: Catalyst: NPC = 0.1 g/L, PDS = 0.8 Mm, NBT = 0.25 µM, temp =

25°C, shake: 150 rpm

NOTE: As shown in Figure S17 and 4a, monoformazan was not detected at 530 nm by UV spectrophotometer, [7] which indicated that $O_2^{\cdot-}$ were not present in both ZnO@NPC/PDS and NPC/PDS systems. In contrast, the decrease in the concentration of NBT may be attributed to the oxidation of NBT by PDS.
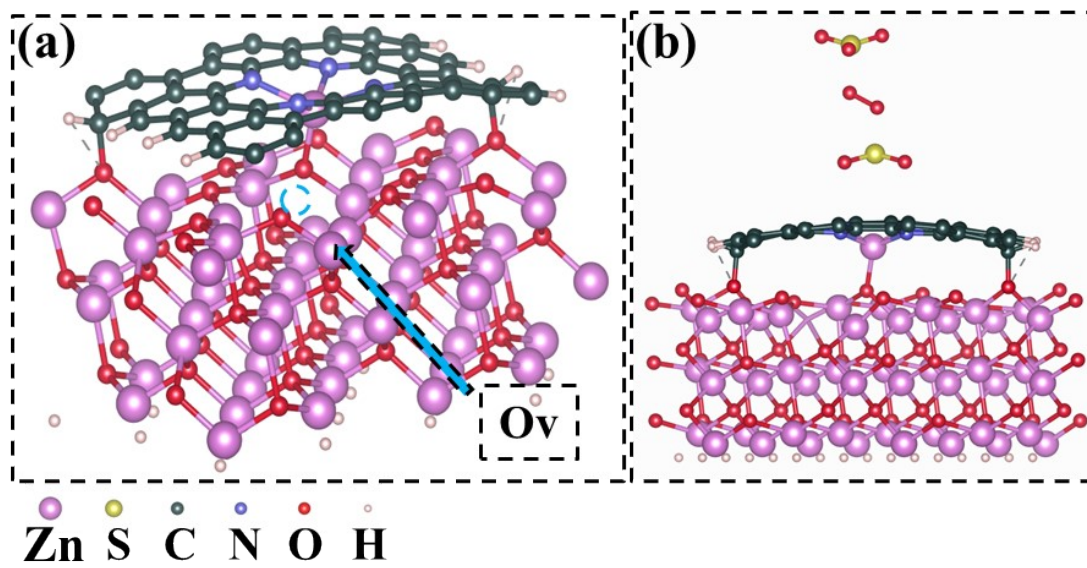
Figure S17: K_{obs} of ZnO@NPC-Etch and N 1s
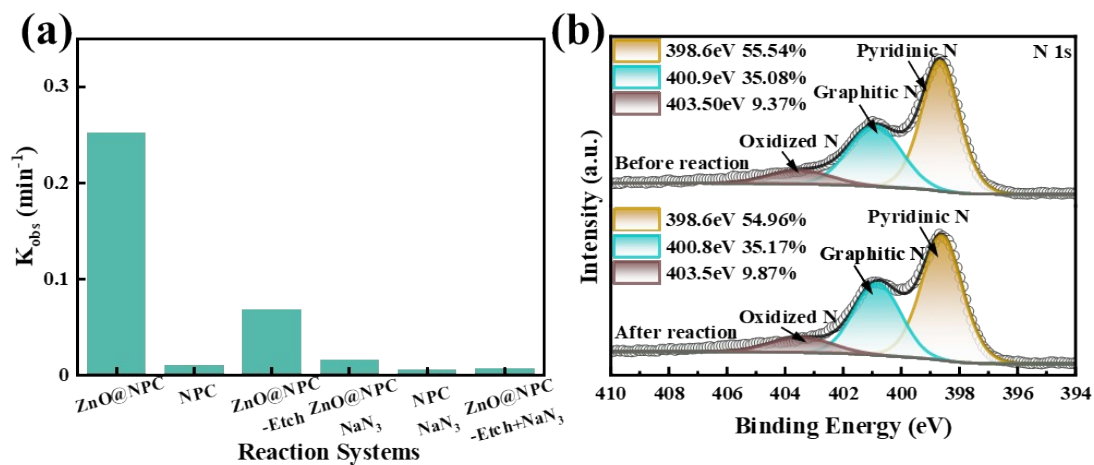
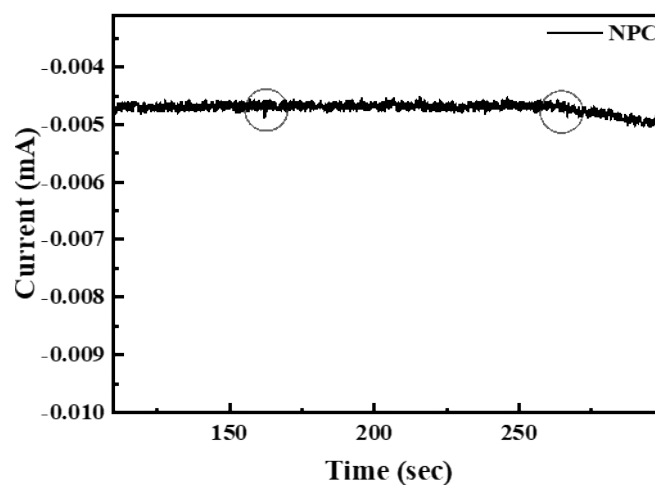(a) K_{obs} of different reaction systems, (b) N 1s of ZnO@NPC before and after the reaction

Figure S18: DFT
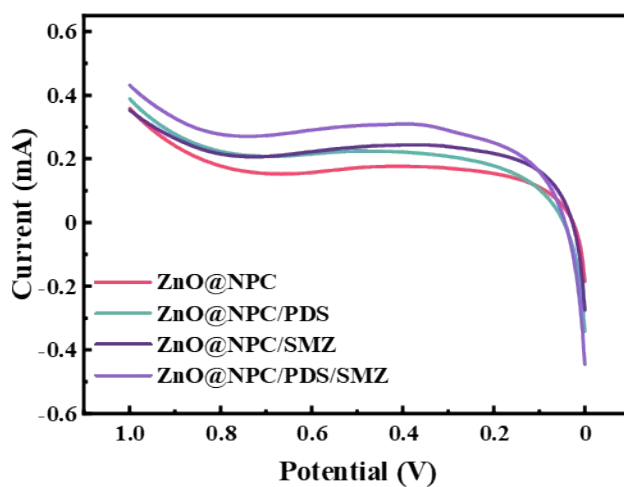

(a) material model, (b) PDS decomposition

Figure S19: I-t curves of NPC

NOTE: Detailed plot of the i-t curve of NPC showed a weak current change with the addition

of PDS and SMZ, indicating the weak electron transfer capacity of NPC.

Figure S20: Linear sweep voltammetry

NOTE: The LSV showed slight increase in current with the addition of PDS and SMZ, respectively. And the overall current of the system increased significantly with PDS and SMZ coexistence. This result was consistent with the trend of the i-t curve, indicating that ZnO@NPC was involved in the electron transfer during the reaction process.

Figure S21: Installation diagram of GOP
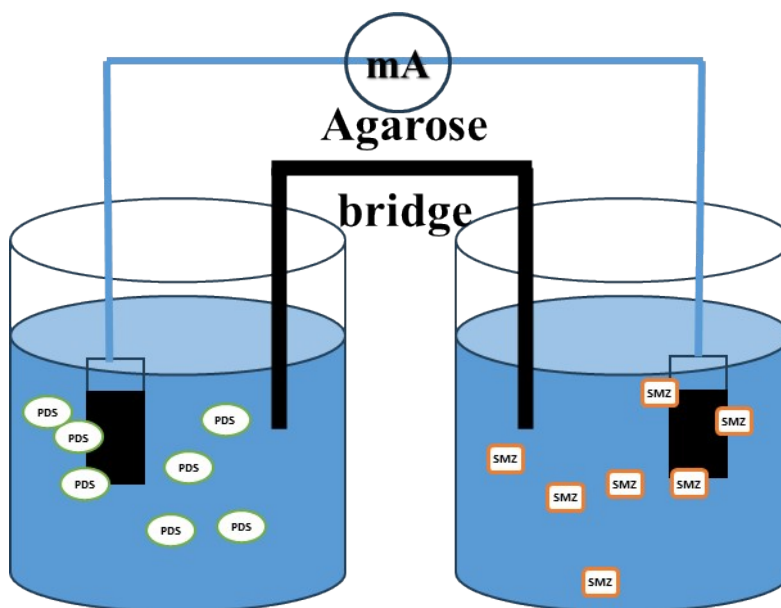
NOTE: The left half-cell is the PDS solution and the right is the SMZ solution, connected with

a salt bridge, and the two working electrodes are connected by an ammeter for detecting the current

in the pathway. The results were shown in Figure 5b and 5c, which recorded the change in current

and pollutant removal during the reaction. This apparatus allowed visualization of current change

and the direction of electron transfer.

Figure S22: Intermediates
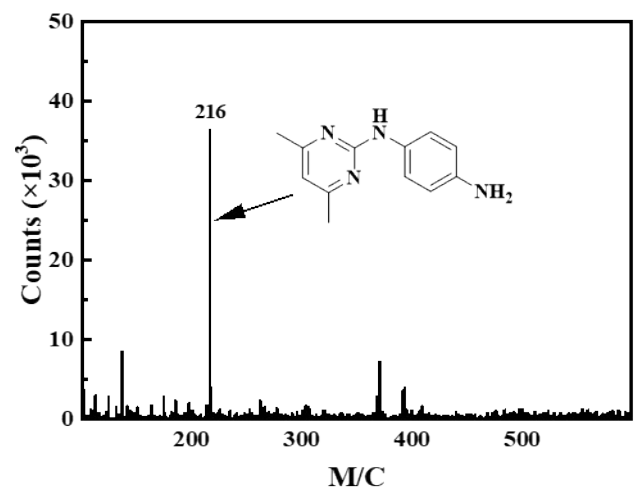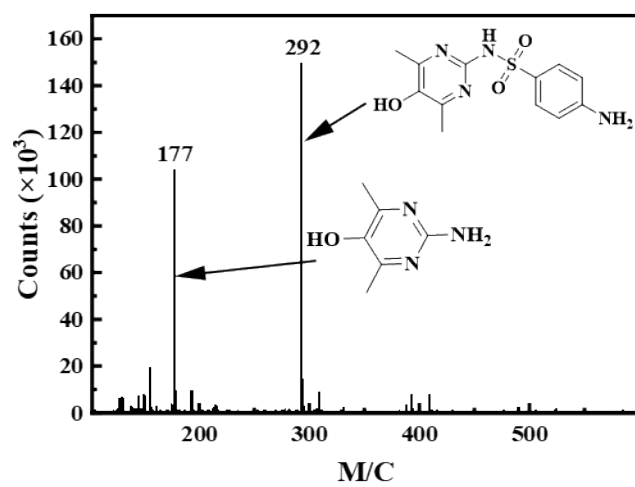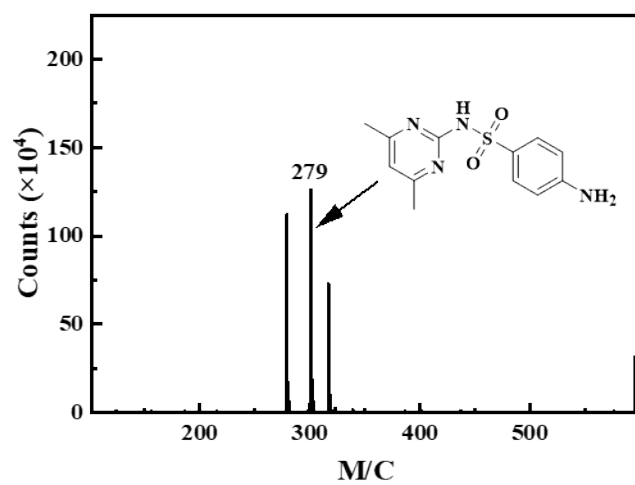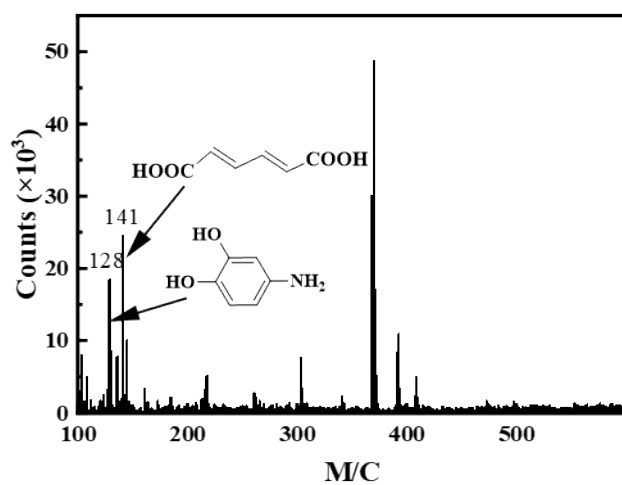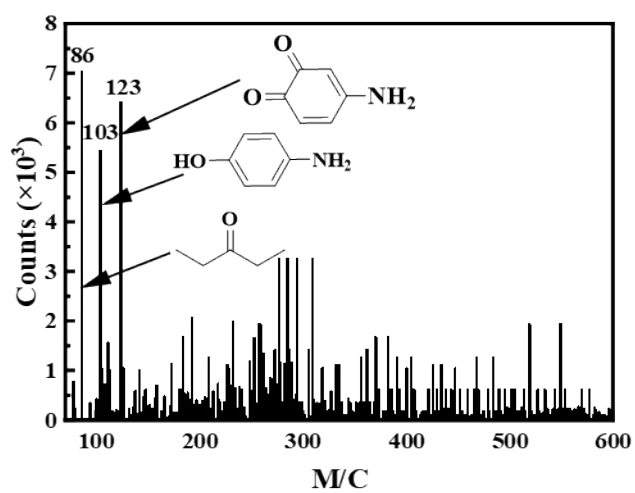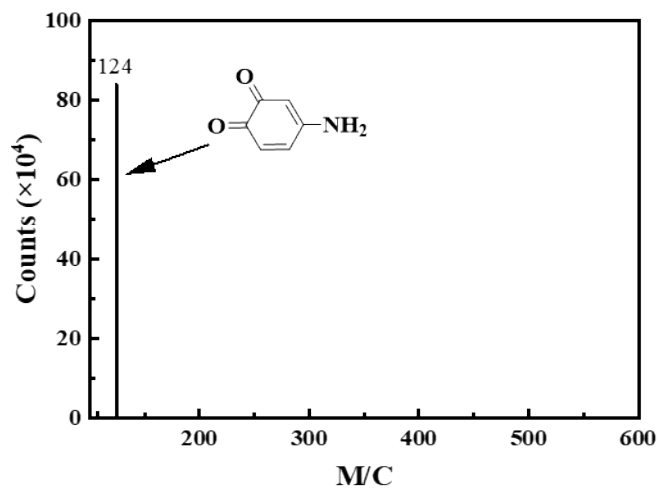
Figure S23: Degradation pathways
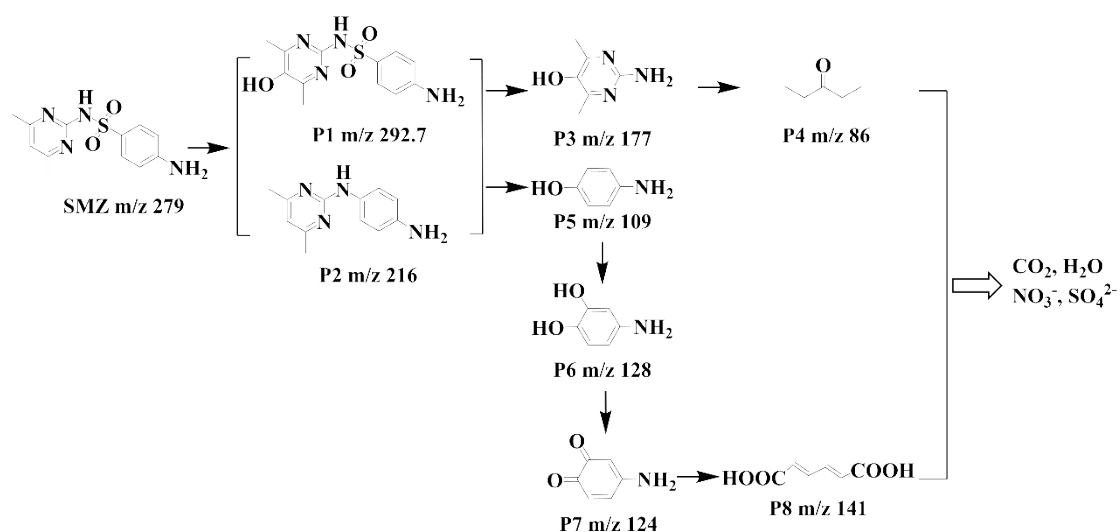
NOTE: Based on the analysis of intermediates, two degradation pathways were proposed in Figure S8. For path one, SMZ was converted to P1 through hydroxylation, P1 was converted to P3 and P5 by SO_2 elimination and breaking the bond. [8] For path two, SMZ was converted to P2 by taking off SO_2, and P2 generated P3 and P5 under the action of $^1O_2$. [9] P3 opened the ring under the attack of $^1O_2$ to form P4 and converted to small molecule organisms with deprotonation. P5 was hydroxylation formed P6, and two other byproducts (P7 and P8) with relatively lower molecular weights which were arose from deprotonated and ring opened. Finally, it is converted into harmless inorganic substances to remove pollutants and reduce total organic carbon.

Figure S24: Changes in toxicity of intermediates
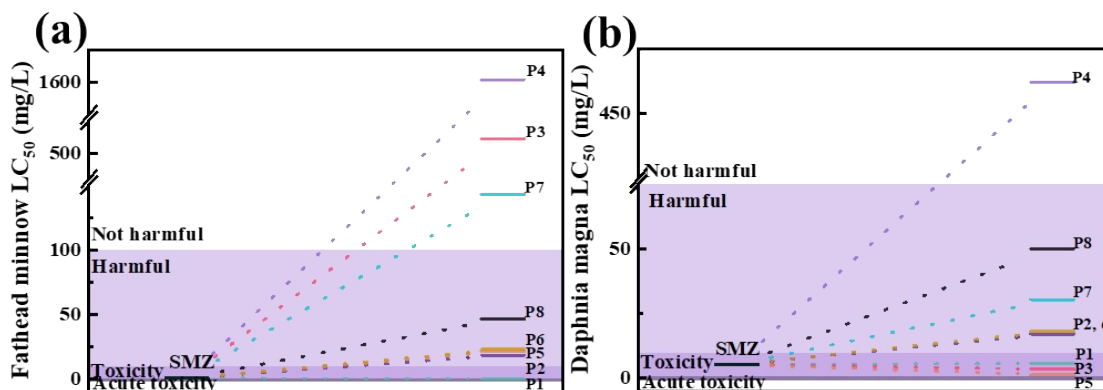
(a) Fathead minnow LC$_{50}$, (b) Daphnia magna LC$_{50}$

The result can be classified as acute toxicity (<1 mg/L), toxicity (1-10 mg/L), harmful (10-100mg/L), not-harmful (>100 mg/L), (refer Globally Harmonized System of Classification and Labelling of Chemicals).

NOTE: As predicted by T.E.S.T, the acute toxicity of degradation intermediates showed a trend to decrease, only a few products formed in the early stage of the reaction increased in toxicity, and as the reaction processed, the toxicity of intermediates became not-harmful. As shown in Table S4, the bioconcentration factors in the table were all low (less than 1000), none of them have bioaccumulation and mutagenicity, and the developmental toxicity was less than SMZ.

Figure S25: Seed germination and radicle elongation tests

Day 1　　　　**Day 2**　　　　**Day 3**

Day 5　　　　**Day 4**
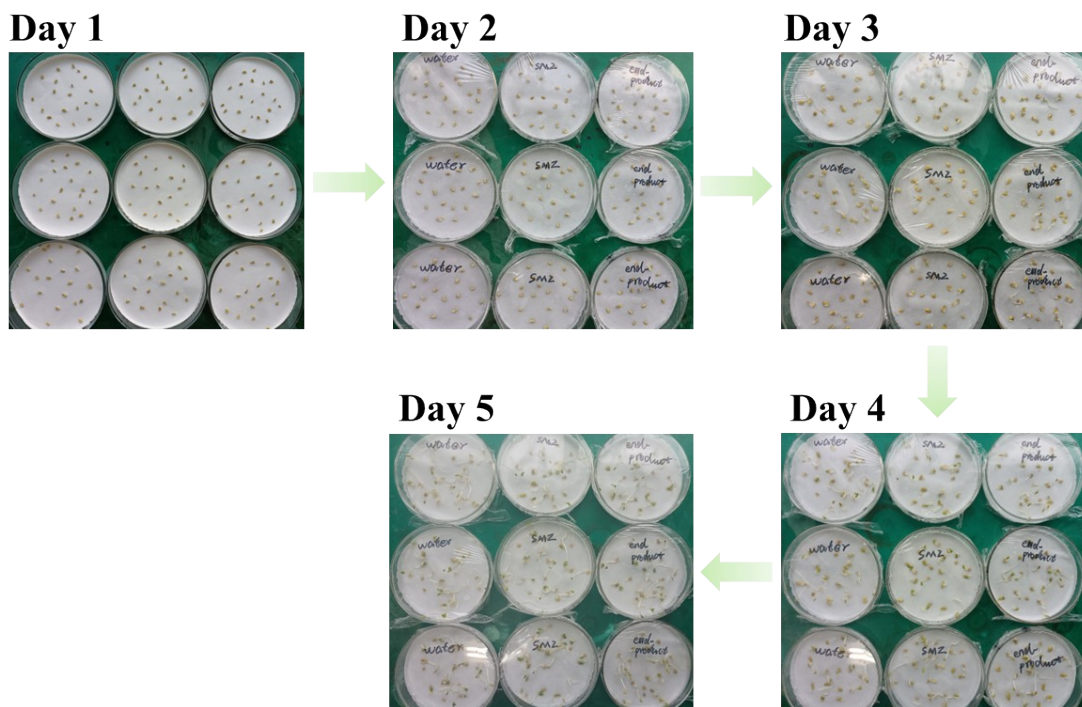
NOTE: The analysis of germination rate and radicle length revealed that all three had a germination rate of about 92%, while the radicle length of SMZ was smaller than that of the other two groups in terms of both the mean and maximum values. Radicle length of lucerne was analyzed by IBM SPSS Statistics 26 software (Table S5), in terms of germination rate, the degradation end-products did not inhibit the germination of seeds. The average length of rhizomes of the three groups was Water > End-product > SMZ, SMZ was the most toxic and had the greatest effect on seeds, while the toxicity of the pollutant solution was greatly reduced after the oxidation reaction. Suggesting that there was no statistical significance in radicle length between watering and watering the degradation end-products, which suggests that the oxidation reaction reduced the toxicity of SMZ.

Figure S26: The different reaction systems in real water
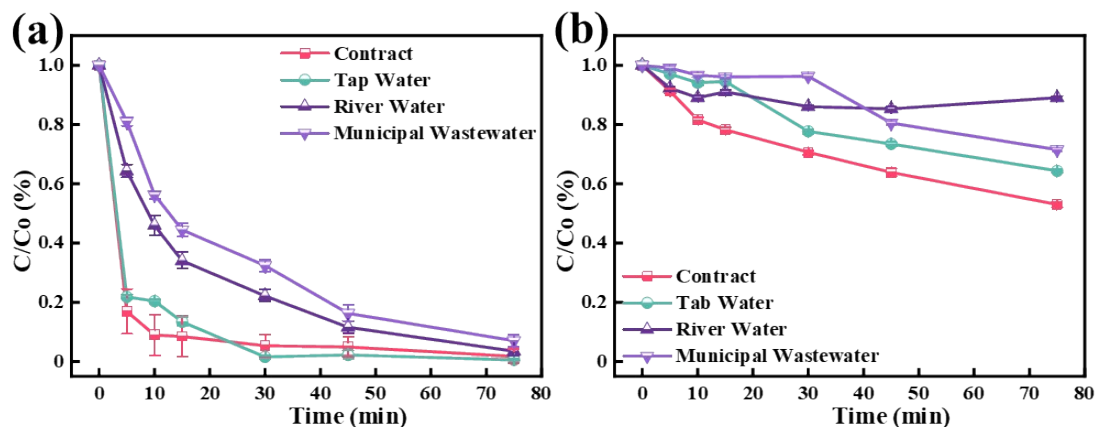
Degradation effect of (a) the ZnO@NPC/PDS system and (b) the NPC/PDS system in real water.

Degradation conditions: Catalyst (ZnO@NPC, NPC) = 100 mg/L, PDS = 0.8 mM, SMZ = 20 mg/L, temp = 25°C, shake 150 rpm

NOTE: From the above application of different catalysts in real water, it could be clearly observed that the ZnO@NPC/PDS system had excellent degradation ability and anti-interference ability. The NPC/PDS system could not remove the pollutants effectively.

Figure S27: Degradation of different pollutants
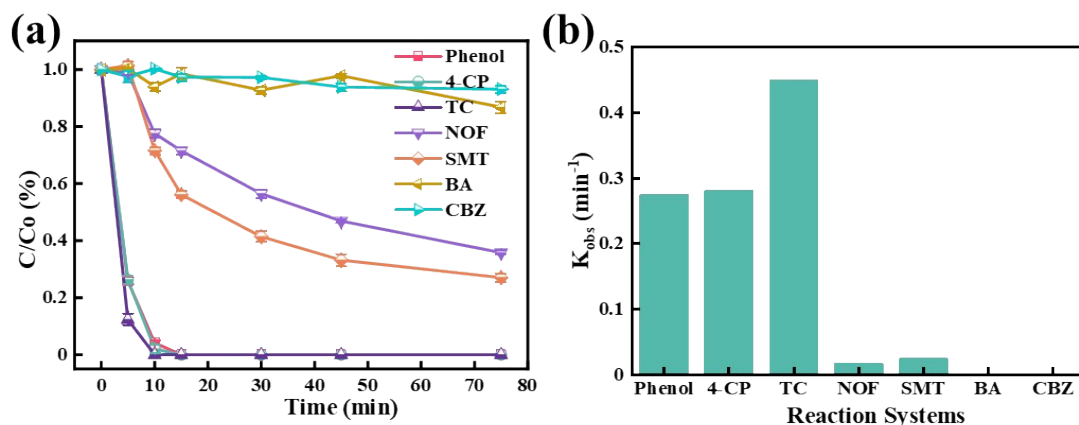
Graph of (a) degradation effect and (b) degradation rate for different pollutants. Degradation condition: catalyst: ZnO@NPC = 0.1 g/L, PDS = 0.8 mM, pollutants (Phenol, 4-CP, TC, NOF, SMT, BA, CBZ) = 20 mg/L, temp = 25°C, shake 150 rpm

NOTE: Eight pollutants were attempted to be degraded in ZnO@NPC/PDS system, Phenol, 4-CP, and TC were rapidly degraded within 10min, NOF and SMT were degraded at a low rate. However, BA and CBZ with electron-withdrawing groups were not degraded, which was consistent with other articles, suggesting $^1O_2$ exhibited strong selectivity for pollutants.

Figure S28: Cycling performance of ZnO@NPC
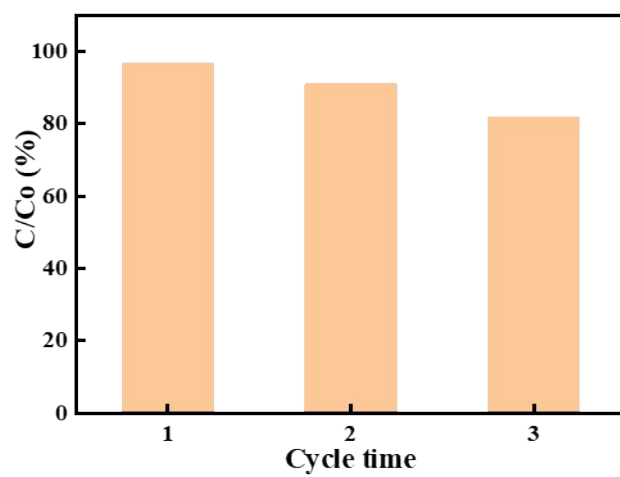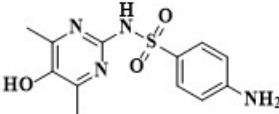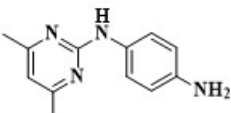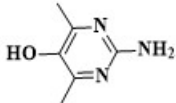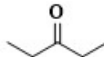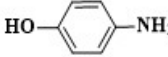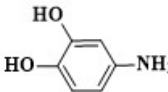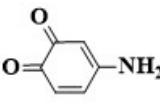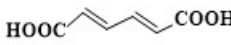
Table S1: The summary of degradation performance in various reported Advanced Oxidation Processes for SAs.

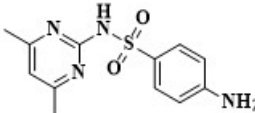| Catalyst	Mass	oxidation	pollutant	Time (min)	Degree (%)	K_{obs} (min^{-1})	Refer
ZnO@NPC	0.1 g/L	PDS 0.8mM	SMZ 20 mg/L	15	90	0.252	This work
C$_v$-CNNs	20 mg/L	Photocatalytic	SDZ 10 mg/L	60	90	0.051	[10]
Fe(Nic)	0.5 g/L	PS 2 mM	SMX 0.04mM	30	90	0.0566	[11]
FCHS	0.2 g/L	PS 2 mM	SDZ 5 mg/L	100	93.5	0.014	[12]
nZVI/OMt	1.5 mM	PDS 1mM	SMZ 20 mg/L	10	60	0.1	[13]
MIP-AA	0.5 g/L	PS 1.88 g/L	SMX 20 mg/L	200	95.1	0.0019	[14]
CuO/SSS	1 g/L	PS 4 mM	SMD 20 mg/L	30	80.29	0.057	[15]
Co$_3$O$_4$ DLHSs	0.1 g/L	PAA 0.4 mM	SAZ 8 mg/L	60	92.2	0.041	[16]
AC	0.1 g/L	PDS 5 mM	SMX 10 mg/L	20	98.2	0.066	
CNT	1 g/L	PDS 5 mM	SMX 10 mg/L	20	69.4	0.020	[17]
CSB-750	0.2 g/L	PS 0.5Mm	SMX 20 mg/L	30	98.7	0.1679	[18]
Co-Fe-Cube	40 mg/L	PAA 100 μM	SMX 10 μM	15	90	0.087	[19]
Fe-CuFe$_2$O$_4$@BC	0.1 g/L	PDS 0.5 mM	SMT 10 mg/L	30	97.76	0.170	[20]
NPBC	0.1 g/L	PDS 0.5 mM	SPY 20 mg/L	120	98.3	0.0342	[21]
5wt%Pr/CN	0.4 g/L	Photocatalytic	SCP 5mg/L	60	98	0.056	[22]

Table S2: The N content of ZnO@NPC before and after reaction

Sample (ZnO@NPC)	N (%)	Pyridinic N (%)	Graphitic N (%)	Oxidized N (%)
Before reaction	11.9	6.6	4.2	1.1
After reaction	11.5	6.7	3.6	1.2

Table S3: Detailed intermediates information.

Sample	Name	m/z	Molecular Formula	Chemical Structure
SMZ	Sulfamethazine	279.0	$C_{12}H_{14}N_4O_2S$	
P1	4-amino-N-(5-hydroxy-4,6-dimethylpyrimidin-2-yl) benzene sulfonamide	292.7	$C_{12}H_{14}N_4O_3S$	
P2	4-N-(4,6-dimethylpyrimidin-2-yl) benzene-1,4-diamine	216.0	$C_{12}H_{14}N_4$	
P3	2-amino-4,6-dimethyl-5-pyrimidinol	177.0	$C_6H_9N_3O$	
P4	pentan-3-one	86.0	$C_5H_{10}O$	
P5	4-aminophenol	109.0	C_6H_7NO	
P6	4-aminobenzene-1,2-diol	128.0	$C_6H_7NO_2$	
P7	4-aminocyclohexa-3,5-diene-1,2-dione	124.0	$C_6H_5NO_2$	
P8	(2E,4E)-hexa-2,4-dienedioic acid	141.0	$C_6H_6O_4$	

Table S4: Toxicity prediction results

Sample	Acute toxicity (LC_{50}) (mg/L)			Bioconcentration factor	Developmental Toxicity	Mutagenicity
	Daphnia magna (48 h)	Fathead minnow (96 h)	T. pyriformis (48 h)			
SMZ	5.44	1.27	6.69	2.57	1	0
P1	5.71	0.21	7.02	1.51	1	0
P2	17.15	18.81	8.79	10.66	0.54	0.67
P3	3.61	510.47	688.61	2.21	0.67	0.33
P4	461.85	1601.39	2062.99	3.76	0.33	0.33
P5	1.37	21.75	17.68	7.04	0.67	0.67
P6	18.08	23.29	122.24	3.24	0.67	0
P7	30.44	142.37	76.46	1.52	0	0.33
P8	50.03	46.69	435.73	0.43	0.33	0

The result can be classified as acute toxicity (<1 mg/L), toxicity (1-10 mg/L), harmful (10-100mg/L), not-harmful (>100 mg/L), (refer Globally Harmonized System of Classification and Labelling of Chemicals), Bioaccumulate (>1000), not Bioaccumulate (<1000)

Table S5: Seed germination and radicle elongation tests

Samples	Seed germination	Germination rate	Radicle elongation	Standard deviation	Minimum	Maximum
Water	56	93.30 %	2.7625	1.99951	0.2	8
SMZ	56	93.30 %	2.3214	1.3416	0.3	6.7
End-product	57	95.00 %	2.4684	1.89239	0.3	9.2

Table S6: Detection method details

Chemical	mobile phase	flow rate (ml/min)	Tem (°C)	wavelength (nm)	Injection volume (μL)
SMZ	acetonitrile/water (35:65 v/v%)	1	30	266	20
SMT	acetonitrile/0.1% HCOOH (45:55 v/v%)	1	30	267	20
TC	acetonitrile/0.1% HCOOH (20:80 v/v%)	1	30	354	20
NOF	acetonitrile/0.15% Phosphoric acid (15:85 v/v%)	1	30	279	20
Phenol	MeOH/water (45:55 v/v%)	1	30	270	20
4-CP	MeOH/water (70:30 v/v%)	1	30	280	20
BA	acetonitrile/0.1% CH3COOH (50:50 v/v%)	1	30	230	20
CBZ	acetonitrile/0.1% CH3COOH (50:50 v/v%)	1	30	285	20
PMSO	acetonitrile/water (30:70 v/v%)	1	30	230	20
$PMSO_2$	acetonitrile/water (30:70 v/v%)	1	30	215	20

Reference

1. Q. Qi, S. Liu, X. Li, C. Kong, Z. Guo and L. Chen, In situ fabrication of ZnO@N-doped nanoporous carbon core-shell heterostructures with high photocatalytic and adsorption capacity by a calcination of ZnO@MOF strategy, *J. Solid State Chem.*, 2017, **255**, 108-114.

2. X. Song, S. Chen, L. Guo, Y. Sun, X. Li, X. Cao, Z. Wang, J. Sun, C. Lin and Y. Wang, General Dimension-Controlled Synthesis of Hollow Carbon Embedded with Metal Singe

Atoms or Core-Shell Nanoparticles for Energy Storage Applications, *Adv. Energy Mater.*, 2018, **8**.

3.   R. Freund, A. E. Lanza, S. Canossa, M. Gemmi, J. Goscianska, V. Cauda, M. Oschatz and S. Wuttke, Understanding the Chemistry of Metal Oxide to Metal–Organic Framework Reactions for Morphology Control, *Chem. Mater.*, 2023, **35**, 1891-1900.

4.   H. Wang, W. Guo, B. Liu, Q. Si, H. Luo, Q. Zhao and N. Ren, Sludge-derived biochar as efficient persulfate activators: Sulfurization-induced electronic structure modulation and disparate nonradical mechanisms, *Appl. Catal., B*, 2020, **279**.

5.   H. Yang, R. Qiu, Y. Tang, S. Ye, S. Wu, F. Qin, L. Xiang, X. Tan, G. Zeng and M. Yan, Carbonyl and defect of metal-free char trigger electron transfer and $O_2^{\bullet-}$ in persulfate activation for Aniline aerofloat degradation, *Water Res.*, 2023, **231**.

6.   Y. Shang, X. Liu, Y. Li, Y. Gao, B. Gao, X. Xu and Q. Yue, Boosting fenton-like reaction by reconstructed single Fe atom catalyst for oxidizing organics: Synergistic effect of conjugated π-π sp_2 structured carbon and isolated $Fe-N_4$ sites, *Chem. Eng. J.*, 2022, **446**.

7.   B. H. J. Blelski, G. G. Shiue and S. Bajuk, Reduction of Nitro Blue Tetrazolium by $C0_2^-$ and 0_2^- Radicals, *J. Phys. Chem*, 1980, **84**, 830-833.

8.   M. Li, C. Wang, M. Yau, J. R. Bolton and Z. Qiang, Sulfamethazine degradation in water by the VUV/UV process: Kinetics, mechanism and antibacterial activity determination based on a mini-fluidic VUV/UV photoreaction system, *Water Res.*, 2017, **108**, 348-355.

9.   B. Annel, A. William and M. Kristopher, Triplet-sensitized photodegradation of sulfa drugs containing six-membered heterocyclic groups: identification of an SO_2 extrusion photoproduct, *Environ. Sci. Technol*, 2005, **39**, 3630-3638.

10. M. Liu, D. Zhang, J. Han, C. Liu, Y. Ding, Z. Wang and A. Wang, Adsorption enhanced photocatalytic degradation sulfadiazine antibiotic using porous carbon nitride nanosheets with carbon vacancies, *Chem. Eng. J.*, 2020, **382**, 123017.

11. M. Pu, J. Niu, M. L. Brusseau, Y. Sun, C. Zhou, S. Deng and J. Wan, Ferrous metal-organic frameworks with strong electron-donating properties for persulfate activation to effectively degrade aqueous sulfamethoxazole, *Chem. Eng. J.*, 2020, **394**, 125044.

12. T. Liu, K. Wu, M. Wang, C. Jing, Y. Chen, S. Yang and P. Jin, Performance and mechanisms of sulfadiazine removal using persulfate activated by Fe_3O_4@CuOx hollow spheres, *Chemosphere*, 2021, **262**, 127845.

13. M. Li, Z. He, H. Zhong, L. Hu and W. Sun, Multi-walled carbon nanotubes facilitated Roxarsone elimination in SR-AOPs by accelerating electron transfer in modified electrolytic manganese residue and forming surface activated-complexes, *Water Res.*, 2021, **200**, 117266.

14. Y. Xie, J. Wan, Z. Yan, Y. Wang, T. Xiao, J. Hou and H. Chen, Targeted degradation of sulfamethoxazole in wastewater by molecularly imprinted MOFs in advanced oxidation processes: Degradation pathways and mechanism, *Chem. Eng. J.*, 2022, **429**, 132237.

15. K. Yin, L. Hao and G. Li, CuO nanosheets incorporated scrap steel slag coupled with persulfate catalysts for high-efficient degradation of sulfonamide from water, *Environ Res*, 2023, **216**, 114614.

16. J. Wu, X. Zheng, Y. Wang, H. Liu, Y. Wu, X. Jin, P. Chen, W. Lv and G. Liu, Activation of peracetic acid via Co_3O_4 with double-layered hollow structures for the highly efficient removal of sulfonamides: Kinetics insights and assessment of practical applications, *J. Hazard. Mater.*, 2022, **431**, 128579.

17. J. Liang, K. Chen, X. Duan, L. Zhao, H. Qiu, X. Xu and X. Cao, pH-dependent generation of radical and nonradical species for sulfamethoxazole degradation in different carbon/persulfate systems, *Water Res.*, 2022, **224**, 119113.

18. F. Ye, W. Sun, K. Pang, W. Yang, M. Pu and Q. Zhang, Coupling of sulfur and boron in carbonaceous material to strengthen persulfate activation for antibiotic degradation: Active sites, mechanism, and toxicity assessment, *Chin. Chem. Lett.*, 2023, **34**, 107755.

19. Y. Cheng, Z. Wang, L. Cao, Z. Chen, Y. Chen, Z. Liu, J. Ma and P. Xie, Tailorable morphology control of Prussian blue analogues toward efficient peracetic acid activation for sulfonamides removal, *Appl. Catal., B*, 2024, **342**, 123409.

20. Y. Wang, L. Wang, Y. Cao and F. Ma, Oxygen vacancies-enriched Fe-Cu bimetallic minerals-based magnetic biochar activated peroxydisulfate for durable sulfonamides degradation: pH-dependence adsorption and singlet oxygen evolution mechanism, *Sep. Purif. Technol.*, 2023, **317**, 123866.

21. W. Tang, D. S. Alessi, T. Wang, J. Wu, S. Li, K. O. Konhauser, Z. Li and J. Chen, Efficient removal of sulfonamides in complex aqueous environments by an N, P-co-doped graphitic biochar: the crucial role of P2O5, *Green Chem.*, 2024, **26**, 3229-3238.

22. Q. Li, S. He, L. Wang, M. Zhao, T. Guo, X. Ma and Z. Meng, A novel Z-scheme heterojunction g-C3N4/g-C3N4/Pr6O11 for efficient visible-light photocatalytic degradation of sulfonamide, *Appl. Organomet. Chem.*, 2024, **38**, e7344.